We are IntechOpen,
the world's leading publisher of Open Access books
Built by scientists, for scientists

6,100
Open access books available

149,000
International authors and editors

185M
Downloads

154
Countries delivered to

Our authors are among the

TOP 1%
most cited scientists

12.2%
Contributors from top 500 universities

CLARIVATE ANALYTICS
BOOK CITATION INDEX
INDEXED

WEB OF SCIENCE™

Selection of our books indexed in the Book Citation Index
in Web of Science™ Core Collection (BKCI)

Interested in publishing with us?
Contact book.department@intechopen.com

Spaceborne LiDAR Surveying and Mapping

Fang Yong, Zhang Li, Gong Hui, Cao Bincai, Gao Li and Hu Haiyan

Abstract

Laser point cloud data have the characteristics of high elevation accuracy, fast processing efficiency, strong three-dimensional (3D) vision, and wide application fields. It will be one of the core datasets of the new generation national global topographic database. The rapid advancement of spaceborne laser earth observation technology allows the collection of global 3D point cloud data, which has brought a new breakthrough in the field of satellite-based earth observation, and its significant advantages of all-day time, high accuracy and high efficiency will lead the future development of space precise mapping technology. This chapter firstly introduces the principle and development status of satellite-based LiDAR technology, then presents the basic technical framework of satellite-based LiDAR 3D mapping, and analyzes the data processing methods of spaceborne photon point clouds, and finally, focuses on the application research in various fields including precise geolocation of combined with satellite images, fusion of multi-source topographic information, polar mapping, 3D objects reconstruction, and shallow sea topographic mapping, etc.

Keywords: global laser point cloud, global control point library, global 3D elevation data, 3D digital geospatial framework, global topographic database, 3D precise geometric positioning, multi-source topographic information fusion, polar mapping, 3D object reconstruction, shallow sea topographic mapping

1. Introduction

In recent years, LiDAR (Light Detection and Ranging) has been developing rapidly as a new generation of precise earth observation technology. The satellite-based LiDAR system uses satellite as the platform and photon-counting LiDAR as the main payload to detect global surface 3D information around the clock, precisely determine laser point positions in near real time, and simultaneously collect 3D point clouds (active SLAM) in the mission region, as shown in **Figure 1**, providing a new and efficient means to rapidly implement global 3D information mapping (including:
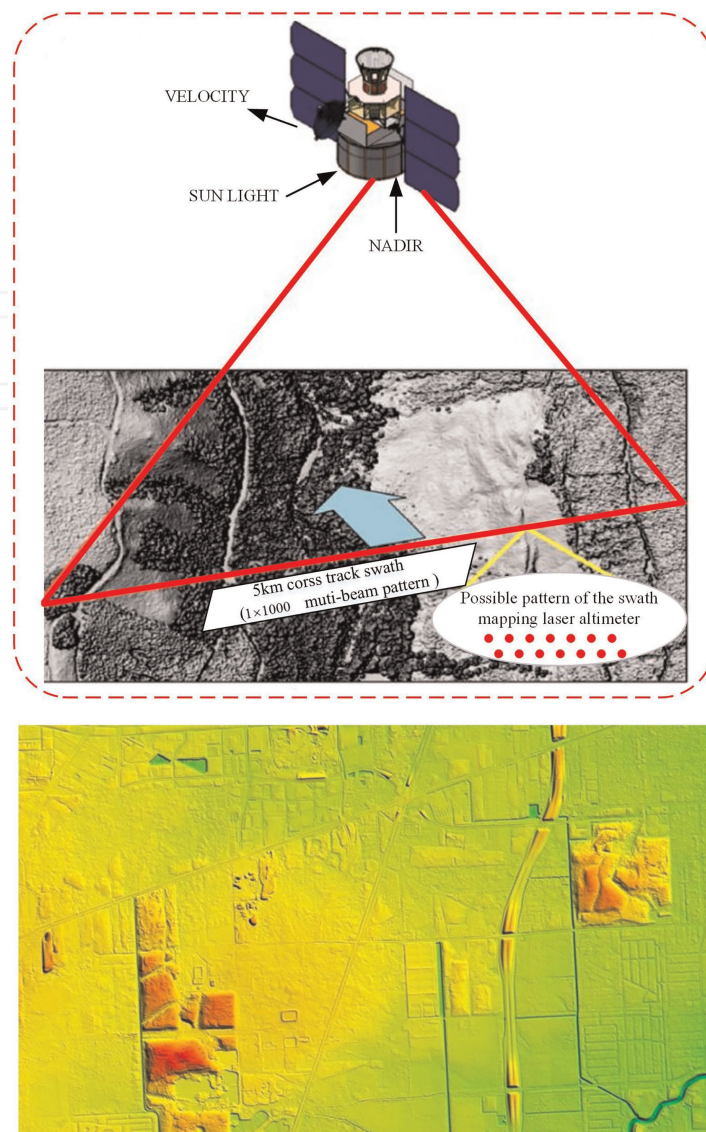
Figure 1.
Schematic diagram of satellite-based LiDAR measurement. (TOP: LIST satellite for example; Bottom: DSM).

high-precision laser control points, 3D digital surface model (DSM), and digital elevation model (DEM)).

Compared with the existing or developing optical or microwave remote sensing mapping satellites, it has the advantages of high accuracy of observation data and fast information acquisition efficiency. First, the elevation accuracy is improved by 5–10 times; second, the data processing is highly automated; and third, the overall acquisition cost is significantly reduced. The development of satellite-based LiDAR measurement means can effectively improve the overall geometric accuracy of earth observation, provide basic 3D topographic data support for the comprehensive application of various types of remote sensing satellite images; fill in the gaps of geospatial information in the polar regions; and provide high-precision 3D frame information support for precise location services [1–8].

The rapid development of satellite-based LiDAR measurement technology has brought a new breakthrough in the field of satellite-based earth observation, and the significant advantages of all-day, high-precision and high-efficiency will definitely lead the future development direction of aerospace remote sensing and mapping technology [5].

2. Principle and development status of satellite-based LiDAR technology

2.1 Basic principle

The satellite-based LiDAR measurement is performed by transmitting laser pulses at a certain frequency from the satellite-based laser to the ground, and the laser beam crosses the atmosphere and is scattered by the terrain surface, producing a weak backscattered echo, which is received by the telescope on the satellite-based LiDAR, and the distance value between the laser and the detection target is calculated through photoelectric signal conversion and time measurement, and then combined with the information of satellite attitude, platform position, and laser pointing to finally obtain precise three-dimensional spatial coordinates of the laser footprint point, as shown in **Figure 2**. The satellite-based LiDAR measurement belongs to the direct active acquisition of surface elevation information, which is different from the traditional indirect reconstruction measurement mode of remote sensing imaging mapping, reducing the time of post-processing process and improving the efficiency of surface 3D information acquisition.

2.2 Status of development

Satellite-based laser measurement equipment was first used in deep space exploration, such as Apollo-15, 16, 17 (1970, Moon), Clementine (1994, Moon), MGS (1996, Mars), LRO (2009, Moon), OSIRIS (2016, asteroids), Japan SELENE (2007, Moon), Chinese CE-1, 2, 3, 4 (since 2007, Moon) [9], mainly used for surface topography measurements and landing site selection. Due to the large differences between deep space exploration and earth observation in terms of detection environment and accuracy requirements [10, 11], this paper only focuses on earth observation LiDAR systems. As shown in **Table 1**, the existing and planned LiDAR systems for earth observation at worldwide [5, 12–16] mainly include SLA, ICESat, ICESat-2, ZY3–02, GF-7, terrestrial ecosystem carbon monitoring satellite, GEDI, and LIST.

NASA launched the first laser measurement satellite, the Ice, Cloud, and Land Elevation Satellite (ICESat-1), in January 2003, with the Geoscience Laser Altimeter System (GLAS) as the primary payload, with the main mission of measuring land
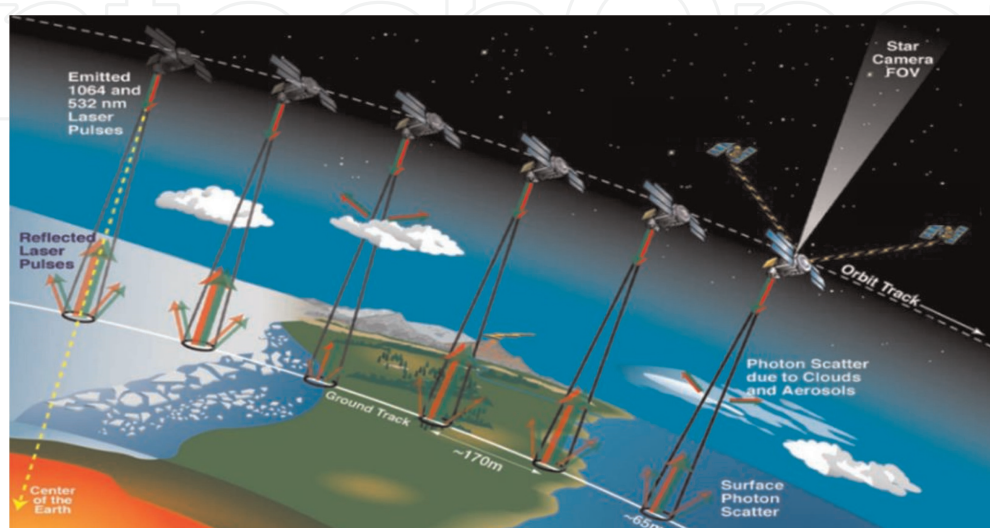

Figure 2.
Principal diagram of satellite-based LiDAR measurement.

Satellite/Payload	Time	Country	Detection mode	Beams	Pulse width (ns)	Sampling distance (m)	Size of footprint (m)	Elevation accuracy (m)	Applications
SLA-01/02	1996/97	US	Pulse	1	10	750	100	1.5	Global Elevation Control Points
ICESat/GLAS	2003	US	Pulse	1	6	170	70	0.15	Sea ice, atmosphere, land, vegetation, etc.
ZY3–02	2016	China	Pulse	1	7	3500	50	1.0	Experimental altimetry
ICESat-2/ ATLAS	2018	US	Photon counting	6	1.5	0.7	<17.5	0.1	Polar regions, ice sheets, atmosphere, land, vegetation, oceans, etc.
GEDI	2018	US	Pulse	8	14	60	25	1.0	Forest Biomass Monitoring
GF-7	2019	China	Pulse	2	4–8	2900	30	1.0	Generalized Elevation Control Point
Terrestrial Ecosystem Carbon Monitoring Satellite	2022	China	Pulse	5	7	200	25–30	1.0	Forestry carbon inventory monitoring, generalized elevation control points
LIST	To be launched	US	Photon counting	1000	1	0.7	5	0.1	Global Digital Elevation Model

Table 1.
Main technical specifications and applications of earth observation laser altimetry instruments at worldwide.
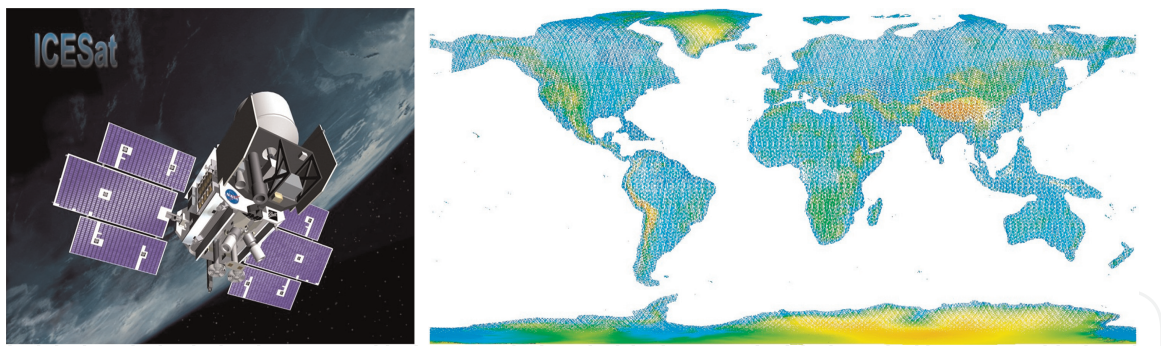
Figure 3.
ICESat and its global laser point cloud data (395 million points, 1.36 GB).

topography, cloud height and vertical structure, and polar ice caps [17]. During its 6.5 years of operation, the ICESat-1 laser altimeter has acquired a large amount of high-precision surface data of the earth, as shown in **Figure 3**, providing a valuable data source for scientific research and practical applications in many fields [18, 19]. Of particular note in the field of global mapping is the ability of surface elevation measurements to construct accurate medium-resolution digital elevation models of the Earth or to combine with optical stereo mapping/InSAR mapping satellite results to significantly improve the elevation accuracy of 3D terrain models [20]. Several studies have shown that the surface laser points acquired by ICESat-1 can be used as auxiliary control data [21, 22], and its elevation measurement accuracy reaches 0.1 m magnitude, which significantly improves the accuracy of aerotriangulation and mapping under uncontrolled conditions, especially in the elevation accuracy [23]. China has added similar laser altimeter payloads to the newly developed Gaofen 7 and Gaofen 14 high-precision stereo mapping satellites [24, 25], which provide support to ensure the accuracy of 1:10,000 scale elevation surveying under satellite conditions.

Given the outstanding performance of the ICESat-1 satellite, the follow-on ICESat-2 laser measurement satellite mission became one of the highest priority satellite observation missions recommended by the National Research Council for the period 2010–2020 [26]. ICESat-2 was successfully launched in September 2018 with a primary payload of the Advanced Topographic Laser Altimeter System (ATLAS), which adopts a photon-counting, high-frequency, micro-pulse, multi-beam laser measurement scheme with a 17 m footprint on the ground and a sampling interval of 0.7 m in the along-track direction. As shown in **Figure 4**, the accuracy and reliability of the earth observation results have been greatly improved compared with the 70 m footprint and 167 m along-track sampling interval of ICESAT-1 [27, 28]. In the 2 years of ICESAT-2 operation, the global surface data collection density is 70 cm apart in the along-track direction, and the maximum spacing is less than 2 km in the vertical track direction on the equator, which provides the possibility to construct a topographic elevation model with higher plane accuracy and resolution from regional to global scales.

The planned launches of laser earth observation satellites are the Terrestrial Ecosystem Carbon Monitoring Satellite (TECMS) and the U.S. LIST (LiDAR Surface Topography) program. The carbon monitoring satellite is the first satellite mainly serving forestry in China, carrying LiDAR and high-resolution multi-angle multispectral cameras to achieve forest height and biomass inversion through synoptic measurements; LIST is proposed to use photon counting detection system to obtain global topographic information of 5 m grid size and 10 cm elevation accuracy with 1000 beams, as well as surface elevation changes of forests, lakes, and ice caps [29].
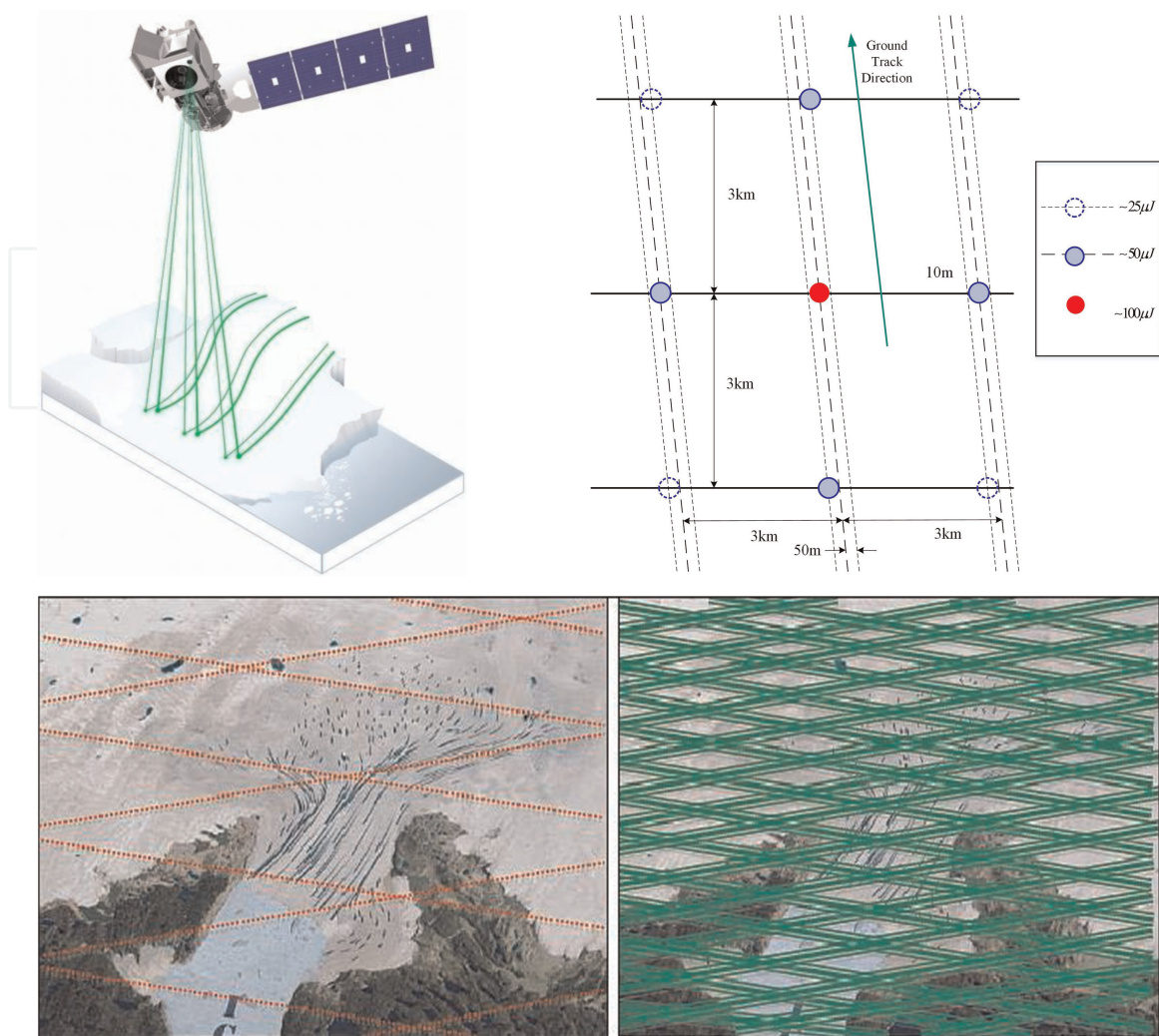
Figure 4.
ICESat-2 satellite, ground beam geometry, comparison of GLAS and ATLAS laser footprint distribution (1500 times higher sampling density).

The satellite-borne high-resolution Earth observation LiDAR is still a very cutting-edge engineering research direction internationally, and foreign research institutions, including the United States, have taken it as an important research content and development direction for future Earth observation. NASA's 20-year development plan for laser imaging radar satellites is shown in the **Figure 5**.

3. Basic technical framework of spaceborne LiDAR 3D mapping

The preferred approach to the acquisition of global laser point cloud data is to use spaceborne instruments. Since the beginning of the twentieth century, two generations of satellite-based LiDAR measurement technology have been developed [30, 31]: the first generation is represented by ICESAT-1, which uses a laser linear detection regime characterized by high-energy pulses, full waveform detection, and high accuracy of elevation measurement to the decimeter level [32]. Limited by the volume of power consumption, it is generally a single beam or several beams with a large laser footprint, which to some extent affects the planimetric positioning accuracy to about 10 m [33]; at the same time, the sampling frequency is low, generally 2–3 Hz, and the density of acquisition points is low, which requires long-period continuous
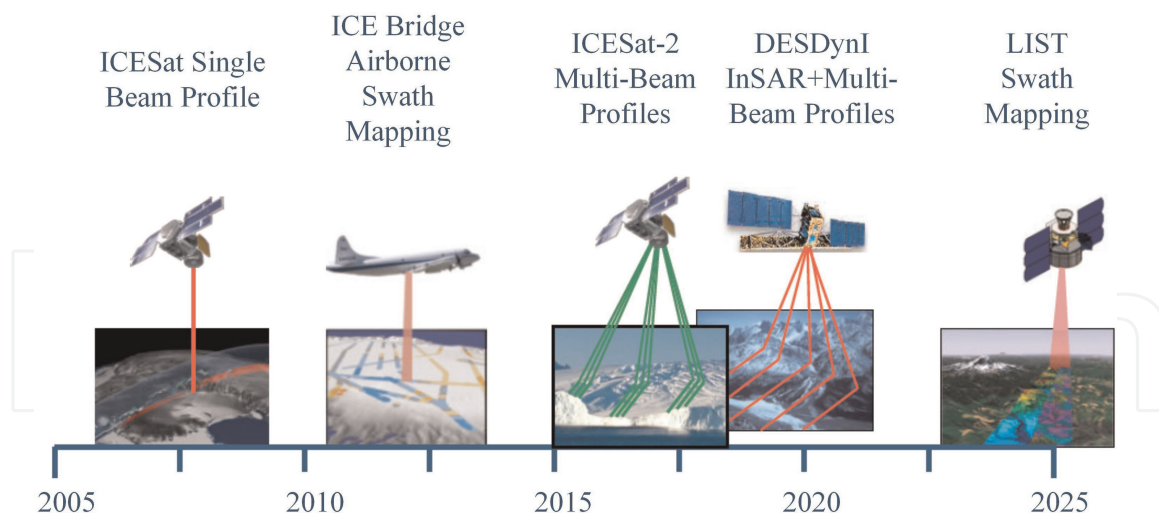
Figure 5.
NASA's 20-year development plan for laser imaging radar satellites.

observation to achieve dense global coverage. The second generation, represented by ICESAT-2, adopts a photon-counting laser detection system [34, 35], characterized by micro-pulse and multi-beam detection, which improves the detection effectiveness by three orders of magnitude while maintaining high accuracy of elevation measurement, and significantly increases the sampling frequency and data sampling density, providing an effective technical way to achieve global high-precision and high-density 3D point cloud data acquisition [28]. With the support of the National Major Science and Technology Project "High Resolution Earth Observation System," China has broken through the key technology of second-generation satellite-based LiDAR measurement after more than 10 years, which has laid a solid foundation for the development of independent laser mapping satellites.

Figure 6 shows the basic technology framework for rapid construction of 3D digital geospatial information based on global laser point cloud. The framework
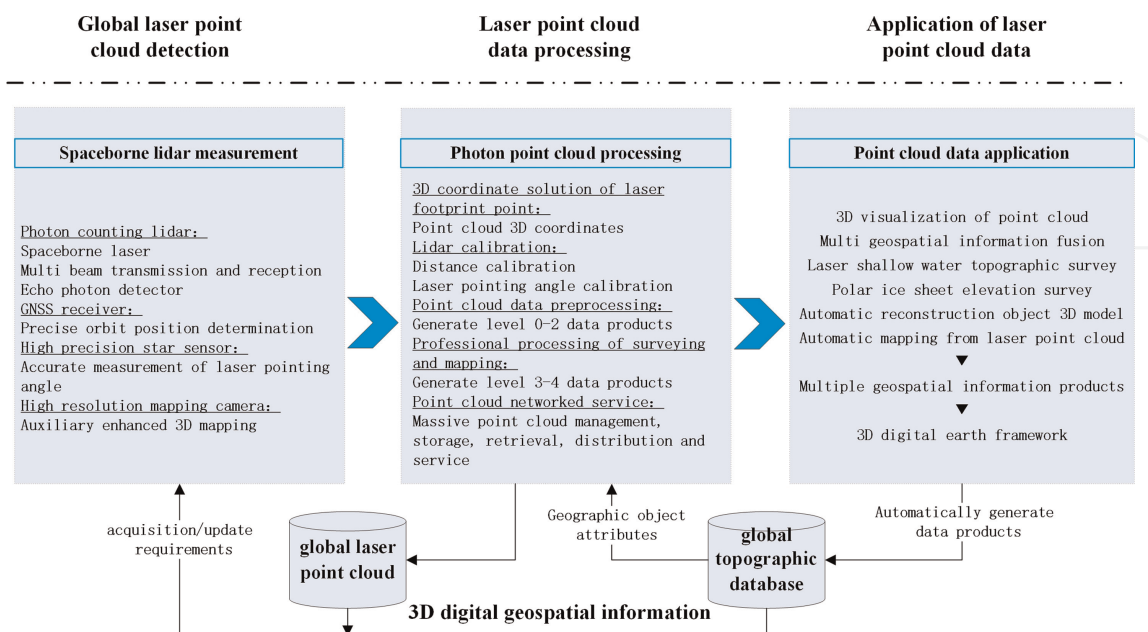

Figure 6.
The setup diagram of 3D digital geospatial information framework to rapid reconstruct based on global laser point cloud.

system mainly includes three parts: global photonic laser point cloud data acquisition, data processing and data application, and the ultimate goal is to form a global point cloud database to support the construction and update of global mapping database.

3.1 Global laser point cloud acquisition

The satellite-based LiDAR measurement is performed by transmitting laser pulses at a certain frequency from the satellite-based laser to the ground, and the laser beam crosses the atmosphere and is scattered by the ground surface, producing a weak backscattered echo, which is received by the telescope on the satellite-based LiDAR, and the distance value between the laser and the detected ground surface is calculated through photoelectric signal conversion and time measurement, and then combined with the satellite attitude, platform position, laser pointing, and other information to finally obtain precise 3D spatial coordinates of the laser footprint point. It mainly involves the key technologies such as long-life on-board laser, multi-beam laser transmission and reception, photon level signal detection, precision orbit position determination, laser pointing accuracy determination, and joint active-passive 3D measurement. The major key technologies involved are long-life on-board laser, multi-beam laser transmission and reception, photon level signal detection, precision orbital position determination, precise determination of laser pointing, and joint active-passive 3D measurement, etc. The technology is characterized by the requirement of laser pointing accuracy to subangular second level and distance measurement accuracy to centimeter level at working altitude of hundreds of kilometers and the realization of 3D coordinate measurement accuracy of laser footprint points on the plane to meter level and elevation to decimeter level. Meanwhile, in order to improve the efficiency and accuracy of global mapping, it adopts a new system of photon counting LiDAR, which reduces the laser footprint size from tens and dozens of meters to the meter level and increases the sampling frequency from a few Hz to 10,000 Hz, improving the detection effectiveness by thousands of times compared with the traditional linear detective system, providing support for the rapid acquisition of high-density and high-quality point clouds. Unlike the traditional optical or microwave remote sensing mapping through the indirect measurement mode by the imaging to achieve three-dimensional reconstruction, the satellite-based LiDAR measurement belongs to the direct active acquisition of surface elevation information, which reduce the post-processing steps and improves the overall efficiency of surface three-dimensional information acquisition.

3.2 Point cloud data processing

According to the photonic point cloud data processing process, the product definition design can be divided into five levels, mainly including original telemetry data (level 0), format decoding data (level 1), point cloud geolocation data (level 2), standard data products (level 3), and thematic data products (level 4), of which levels 0–2 are pre-processing products and levels 3–4 are professional processing products, involving the main technical processes including laser foot point 3D coordinate solution, LiDAR ranging and pointing parameters ground calibration, point cloud data pre-processing, mapping professional processing and networking services. Level 1 processing is to decode the raw package data, format conversion, and data cataloging to obtain the standard format data. The raw standard format data include photon time-of-flight data obtained after instrument delay and other corrections, laser

emission position, and pointing data obtained using precision positional data and calibration data. Level 2 processing is to obtain the laser footprint longitude, latitude, and elevation values, and denoising and pre-classifying the point cloud [36], including (2A) un-noised point cloud and (2B) denoised point cloud. Level 3 processing is to obtain control point data, target area DSM, and polar DSM products after adjustment and gridding, including (3A) control point data, (3B) DSM, (3C) DEM, and (3D) object 3D model. Level 4 processing is for specific application needs, fusion of optical, microwave images and DSM, and other multi-source data to generate thematic products for specific applications, as well as extraction of polar ice cover, atmosphere, vegetation, lakes, and other information in point clouds, and other corresponding thematic products are obtained through specialized professional processing of mapping.

3.3 Point cloud data applications

As a direct digital representation of the global 3D physical world, laser point clouds have been applied in a wide range of directions [37–41], mainly including massive global laser point cloud 3D visualization, multiple terrain information fusion, shallow sea topography, polar elevation measurement, automatic 3D reconstruction of objects, and digital mapping based on point clouds, etc., to realize diverse spatial information product making and provide support for the construction of 3D digital earth framework. Efficient storage management retrieval and visualization of massive point cloud data are the most direct and effective applications. At present, there are successful solutions to support the storage management and visualization application of 3D point clouds with a global data volume of 100 petabytes, such as Bentley Pointools [42] and Euclideon udStream [43], whose 3D engine has the characteristics of loading unlimited spatial data in seconds to achieve rapid application. Secondly, point cloud control surveying realizes multi-source observation data fusion application. Cloud control photogrammetry has been realized in a number of system construction and engineering applications, point cloud support for multi-source terrain information, and three-dimensional model fusion will be the next important research direction, to provide an effective way to quickly establish a large range of consistent accuracy, more rich information-type three-dimensional geospatial information framework. In addition, point cloud mapping to achieve automatic acquisition of 3D information from laser point clouds and transformation into geographic entity representation with structure and function has become a major application direction. Dense point cloud and fully automatic processing can be applied to urban 3D modeling, coastal zone topographic survey, polar elevation mapping, road infrastructure maintenance monitoring, and forest resources survey, etc. It generates multifaceted geospatial information products including 3D models of buildings, digital ground models and digital surface models, forestry thematic products, etc., which can provide support for global mapping database construction and thematic element information update.

4. Data processing methods

4.1 Photon geolocation

The basic principle of satellite-based laser measurement and geometric positioning is that the laser beam is transmitted by the satellite and received by the satellite after reflection from the ground, and the time interval between the laser transmission and

reception t is calculated. The propagation speed of light is c, and the one-way transmission distance of the laser is $\rho = ct/2$, and the three-dimensional coordinates of the laser footprint can be obtained by combining the satellite position and attitude information obtained from the GNSS positioning instrument and the star sensor on board the satellite [44]. The rigorous geometric model is shown in **Figure 7**, where P_{laser} is the reference point of laser emission, P_{GNSS} is the GNSS phase center, O_{Body} is the satellite center of mass, and P_{Ground} is the laser ground footprint (Bounce Point Location).

Laser footprints were precisely geolocated and point clouds were generated using on-orbit calibrated laser ranging parameters, laser pointing parameters, and precision attitude/orbit data, taking into account geophysical corrections such as atmospheric delays and tides. The rigorous geometric location equation for satellite-based LiDAR is as follows:

$$
\begin{pmatrix} X_{\text{spot}} \\ Y_{\text{spot}} \\ Z_{\text{spot}} \end{pmatrix}_{\text{ITRF}} = \begin{pmatrix} X_s \\ Y_s \\ Z_s \end{pmatrix}_{\text{ITRF}} + R_{\text{ICRF}}^{\text{ITRF}} R_{\text{BOD}}^{\text{ICRF}} \left[\begin{pmatrix} \Delta X_{\text{ref}} \\ \Delta Y_{\text{ref}} \\ \Delta Z_{\text{ref}} \end{pmatrix} + \rho \begin{pmatrix} \sin(\theta + \Delta\theta_{1\_i})\cos\alpha \\ \sin(\theta + \Delta\theta_{1\_i})\sin\alpha \\ \cos(\theta + \Delta\theta_{1\_i}) \end{pmatrix} \right]
$$

$$(1)$$

where $(X_s \ Y_s \ Z_s)_{\text{ITRF}}^T$ is the coordinate of the satellite in the ITRF coordinate system, determined by the precision orbiting system; $(\Delta X_{\text{ref}} \ \Delta Y_{\text{ref}} \ \Delta Z_{\text{ref}})^T$ is the fixed offset from the laser emission reference point to the phase center of the GNSS antenna; θ is the laser exit axis pointing angle, i.e., the angle between the projection of the laser emission direction and the XOY plane of this system and the Z-axis negative direction,
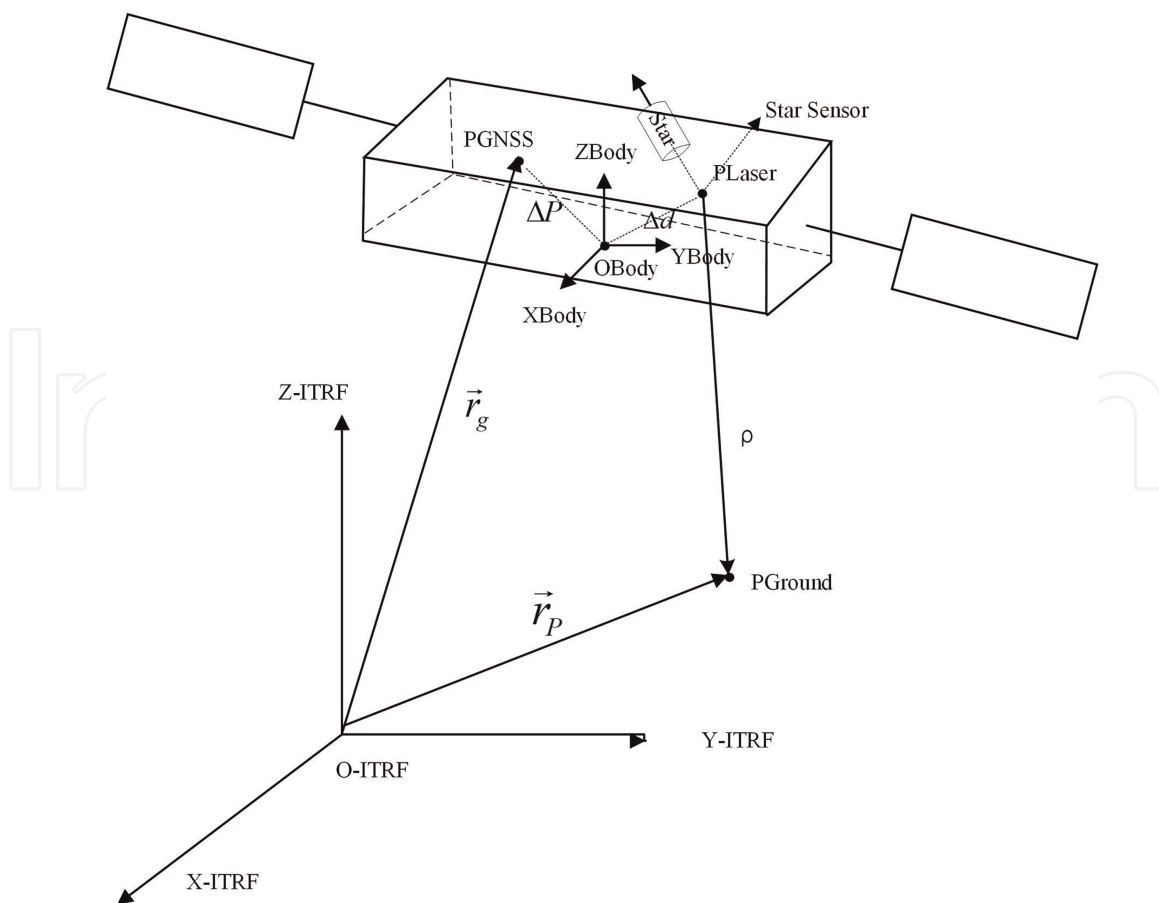

Figure 7.
Schematic diagram of a rigorous geometric positioning model of spaceborne laser point.

α is the angle between the projection of the laser in the XOY plane of this coordinate system and the *X*-axis positive direction; ρ is the laser range value, corrected by the calibration system error and atmospheric delay correction.

Based on the satellite-based LiDAR measurement of the rigorous geometric model, the positioning and elevation calculation of the laser footprint is achieved by the following process:

1. The measured distance is corrected for systematic errors by in-orbit calibration, and then the corrected distance $\rho' = \rho + \Delta\rho_a$ is considered after the atmospheric delay correction $\Delta\rho_a$. The solution of the atmospheric delay depends on the accuracy of the meteorological data. The measured ground data from the Chinese meteorological station and the meteorological data from the GNSS station are interpolated to the NCEP meteorological station coordinates. Since atmospheric corrections have to be performed in real time, continuous validation work is required during the satellite operation to ensure the accuracy of the atmospheric delay correction values.

2. To effectively eliminate the geolocation error caused by optical line difference, the actual position of the laser footprint on the ground is solved using the satellite attitude at the moment of laser emission and the position of the satellite when the laser reaches the ground. According to the laser launch time tT, the satellite attitude data and the laser pointing measurement data are determined from the precision attitude data, and the pointing correction value obtained from the in-orbit calibration is combined to determine the laser pointing in the ICRF coordinate system. Calculating the three-dimensional coordinates of the laser reference point in the ICRF coordinate system and the rotation matrix of the coordinate system from ICRF to ITRF from the precision orbiting data, based on the laser arrival time tm, combined with the fixed offset of the phase center from the laser emission reference point to the GNSS antenna.

3. Calculate the coordinate vector $\begin{pmatrix} X_{\text{spot}} & Y_{\text{spot}} & Z_{\text{spot}} \end{pmatrix}^T_{\text{ITRF}}$ of the laser footprint point in the ITRF coordinate system based on the rigorous geometric model of satellite-based laser altimetry, and then calculate the geodesic coordinates (B, L, H) of the laser footprint point based on the ellipsoidal parameters.

4. Tides include ocean tides, solid tides, etc., whose influence on satellite ranging can reach 0.3–2 m. Therefore, tidal corrections ΔHtide such as ocean tides and solid tides should also be considered to obtain the final coordinates of laser footprints.

Taking ICESat-2 data as an instance, the nominal 6.5 m planimetric positioning accuracy and better than 1 m elevation accuracy were achieved after processing [45]. As shown in **Figure 8**, the evaluation results compared with the airborne DSM data by the iterative least z-difference method in Hanzhong region showed that the horizontal biases of the test data were -0.1 m (east) and -4.1 m (north), and the elevation bias was 0.6 m, which reached the nominal accuracy specifications.

4.2 Photonic point cloud denoising

The extremely high sensitivity of photon-counting LiDAR detection leads to relatively poor data signal-to-noise ratio, and although a narrow-band filter (0.15 nm) is
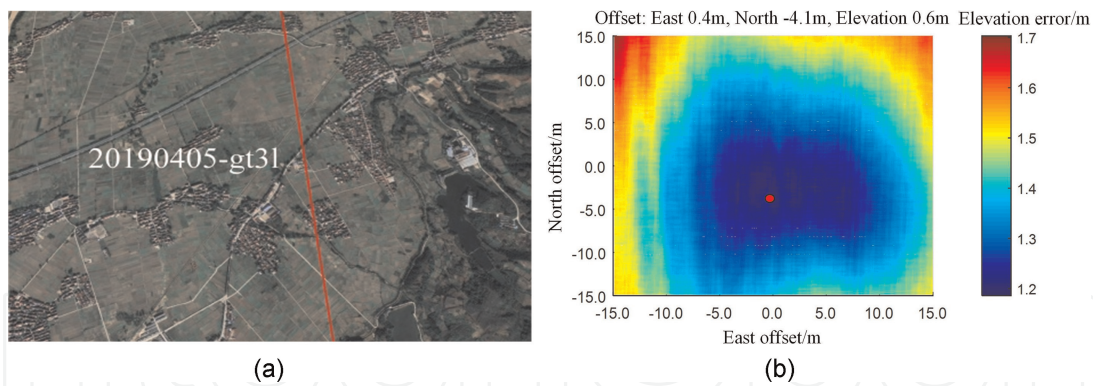
Figure 8.
Accuracy assessment of ICESat-2 using airborne data. (a) Study area; (b) horizontal offset, and red point is best-fitted.

installed, there is still a large amount of background sunlight noise. In some high solar angle and high ground reflectivity scenarios, the background light noise rate reaches about 10 MHz (i.e., 10 million/s, which translates to 1 noise point per 3 m in the elevation direction), so point cloud denoising is critical.

The extremely high sensitivity of photon counting LiDAR detection also leads to a lot of noise and relatively poor signal-to-noise ratio of the data. Although the ICESat-2 receiver is fitted with a narrow-band filter that limits the band range to 532.272 ± 0.15 nm, there is still a large amount of background sunlight in that range. In some high-sun angle and in high ground reflectivity scenarios, the background light noise rate reaches about 10 MHz (i.e., 10 million/s, which translates to 1 noise point per 3 m in the elevation direction) [37], so point cloud denoising is critical.

Most of the currently available photon-counting LiDAR devices record data only along the direction of flight (a swing scan is less common) and therefore are usually processed in a two-dimensional profile. Two denoising algorithms, including the histogram and spatial density methods, are provided in the ICESat-2 basic theory algorithm documents ATL03 [46] and ATL08 [47], respectively: the histogram method considers that the location with the highest number of points in the vertical direction is more likely to be the signal [37]; the spatial density method considers that the signal points are more densely distributed in space, and the density histogram will show the distribution characteristics of "noise on the left, signal on the right" and "high noise and narrow signal" [36]. Based on the "double-peak" distribution of the density histogram, the DRAGANN (Differential, Regressive and Gaussian Adaptive Nearest Neighbor) algorithm is proposed, which uses two Gaussian functions to fit the noise and signal separately and calculates the noise removal threshold adaptively by computing the optimal parameters. The comparison of the two denoising effects is shown in **Figure 9**. The ATL03 algorithm works better in the flat ice cover area, but in the vegetated area, there will be obvious signal point leakage, and ATL08 is more suitable for the vegetated terrain area [48]. In addition, the targeted design on the issues of search kernel shape, terrain correlation, and directional adaptivity can further improve the algorithm performance and obtain better than 98% denoising accuracy [49].

4.3 LiDAR parameters calibration

For a LiDAR measurement satellite similar to ICESat-2 with a 500 km orbital altitude, a pointing angle error of 1 arc second results in a horizontal geolocation error
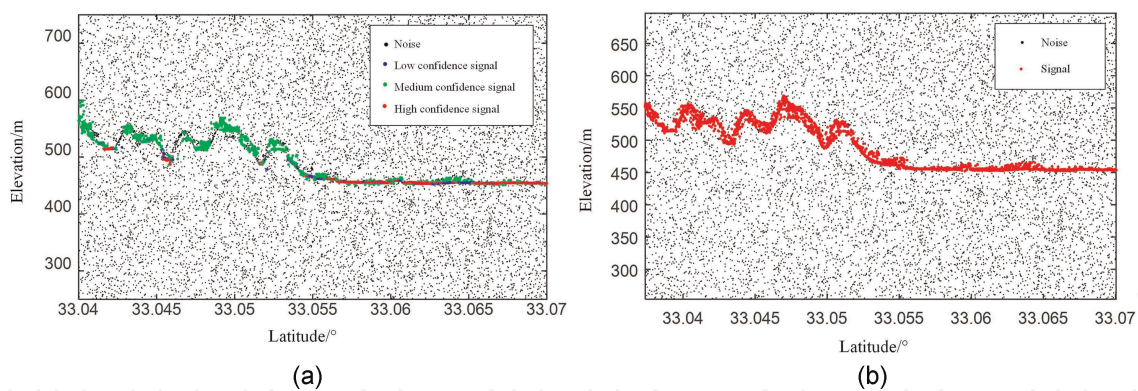
Figure 9.
Comparison of photon counting LiDAR point cloud denoising effects. (a) ATL03 algorithm; (b) ATL08 algorithm.

of about 2.4 m, and an elevation error of 8.3 cm if the ground slope is 2°. Therefore, the rigorous in-orbit calibration of LiDAR work parameters is crucial to the accuracy of elevation measurements.

The on-orbit calibration of satellite-based LiDAR has some similarities with the traditional optical satellite and airborne LiDAR, mainly based on the ground calibration field method or the nature terrain method [50, 51]. The ground-based calibration field directly measures the footprint point through the laser receiver, which has the highest accuracy, but it is necessary to estimate the location of the footprint point and select a suitable location to build the calibration field. The natural terrain method realizes the laser calibration parameter solution by profile alignment with the satellite laser data through the local terrain measured accurately in advance. The rigorous geometric location equation for satellite-based LiDAR is adopted to the basic calibrated model. The iterative pointing angle calibration method was proposed based on the least elevation difference matching criterion. The main steps include two steps: firstly, terrain matching is used to obtain the common terrain feature points whose coordinate deviations are used as input observations, and the second step is to calculate the system calibration parameters by laser beam adjustment. As shown in **Figure 10**, the specific solution can be simplified to calibrate two pointing angular parameters (θ_0, β_0) and 1 range parameter r. It has been shown that the angular calibration accuracy is better than 0.3 arc second using 1 km length laser line matched
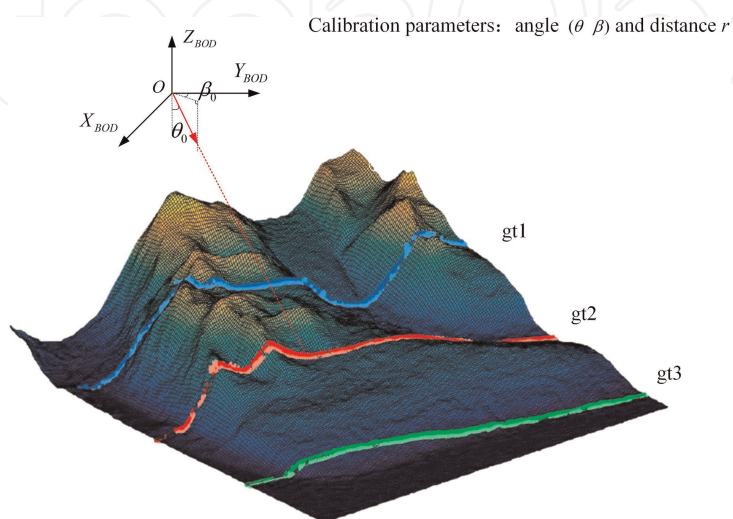

Figure 10.
Diagram of laser on-orbit calibration based on natural terrain.

with high-precision terrain, and the angular calibration accuracy is better than 0.1 arc second when the line length is increased to 2.5 km [52]. In addition, ICESat-2 adopts a similar strategy to ICESat for attitude maneuvering in the oceanic region, and the attitude and distance are calibrated separately by conical scanning, and the long-term drift of the calibrated range values is less than 1 mm/year [53].

5. Application research

5.1 Improve stereo images 3D positioning accuracy

With the characteristics of small ground footprint, high sampling frequency, and large number of beams, the ground observation means of photon counting LiDAR represented by ICESat-2 has greatly improved the planimetric accuracy and flight direction data density of the acquired point cloud, which can be applied as a new 3D control condition to improve the positioning accuracy of satellite images [54–62]. To solve the application problem of photonic point cloud without synchronous image recording plane position, an approach to improve satellite image positioning accuracy with the support of satellite-based photon counting laser point cloud is proposed in this paper; firstly, a 3D terrain profile matching method is used to achieve accurate alignment between photonic point cloud data and DSM automatically generated from satellite stereo image; then terrain feature points are extracted from photonic profile point cloud based on slope change and combined with DSM multiple terrain features to generate common terrain feature control points, and finally introduced into the block adjustment of satellite images with attached parameters as the flat height control condition to further improve the positioning accuracy [63–66]. The experimental results using ZY-3 images and ATLAS ATL03 level data from two regions in Shaanxi Province show that the method can significantly improve the location accuracy without GCPs of satellite images, and compared with the fully uncontrolled positioning and SRTM data-assisted positioning methods, the planimetric and elevation positioning accuracy of ZY-3 image can be further improved by up to 60% and 34%, respectively, which verifies the effectiveness and feasibility of the method [67].

The test data were obtained using ZY-3 satellite images and ICESat-2 ATLAS data in the Xi'an area of Shaanxi Province, China. The ZY-3 satellite image was acquired on April 07, 2019, and the test field contains various types of terrain such as mountains and plains, with elevation relief up to 1200 m. The geographic location of the test area is shown in **Figure 11**, which is a stereoscopic (including front-view, normal-view, and back-view) image area ranging from E108.34°N34.36° to E109.02°N34.92°. The resolution of the front and back view images is 3.5 m, and the normal view image is 2.1 m. The 5-track ATLAS ATL03 data are used, and the acquisition time range is October 26, 2018–January 11, 2021, and the geodetic datum is WGS-84 coordinate system, the plane coordinates are latitude and longitude, and the elevation coordinates are WGS-84 ellipsoidal height, and the distribution on the image is shown in **Figure 11**.

Based on the dense matching using satellite stereo images, the minimum height difference method is used to realize the 3D terrain matching between the photon profiling point cloud and the generated DSM. The basic principle is shown in **Figure 12**, the dashed box is the search range, the solid red-green-blue line is the original three-beam photon point cloud ground track, and the dashed line is the distance search interval of the photon point cloud in its nominated accuracy range. The basic method is to first convert the DSM into regular grid data, take one of the
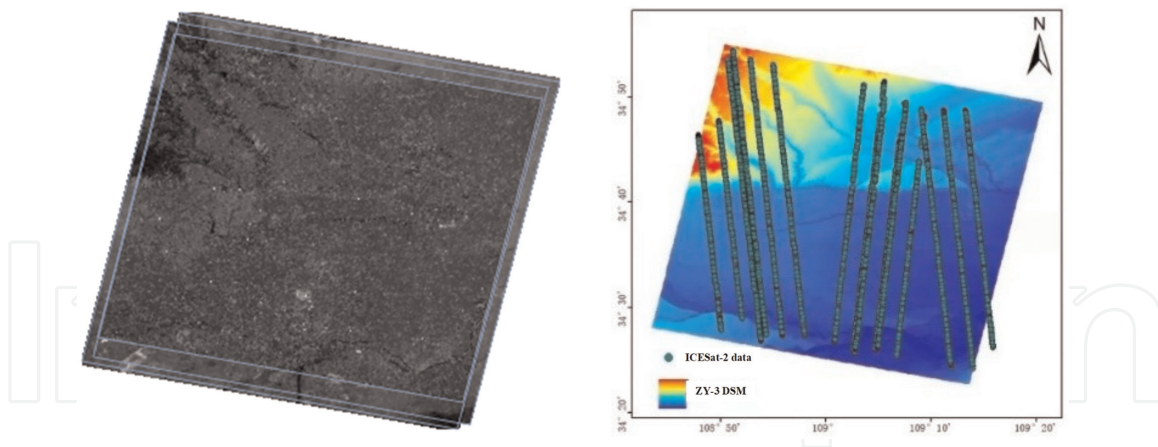
Figure 11.
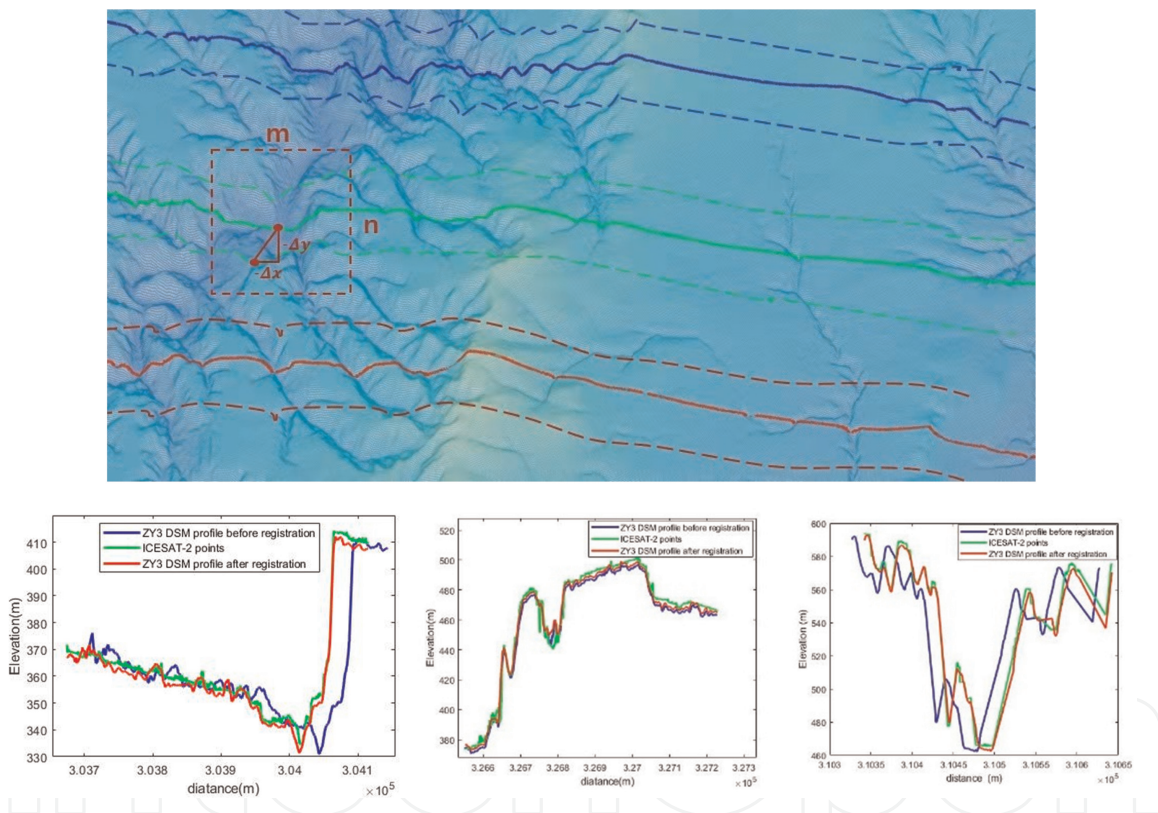*ZY-3 stereo images and ICESat-2 data.*

Figure 12.
Diagram of 3D terrain profile matching between multi-beam photon point cloud and DSM generated by stereo images.

tracks of the multibeam laser point cloud strip as the unit, move in the horizontal or vertical direction with a certain search step Δx or Δy, find the same point of the two data plane coordinates, if there is no corresponding point, use its close interpolation, and then calculate the absolute elevation difference between each laser point and the corresponding plane position of the DSM on multiple strips, until traversing all areas in the step setting area to determine the minimum absolute elevation difference position between corresponding points, which is the plane coordinate position of the profile point cloud matched with DSM.

The principle of terrain matching between profiling laser points and DSM based on the minimum elevation difference method is that the absolute elevation difference between the satellite photon point cloud and DSM in the local range is minimum, the accuracy of laser point cloud is high, and the accuracy of DSM is low, and the offset of the two data relative to the plane position is calculated by elevation constraint. The basic equation is shown as follows.

$$d_{\min} = \text{MIN} \sum_{s=1}^{3} \sum_{l=-m}^{m} \sum_{j=-n}^{n} \left(\sum_{i=1}^{N} |Z_i(X, Y) - h_i(X + l\Delta x, Y + j\Delta y)| \Big/ N \right) \tag{2}$$

In the formula, s is the number of beams, $d_{\min}$ is the absolute value of the elevation difference between the photon point cloud strip and the DSM data generated from satellite images along the profile, N is the number of laser points in the strip, Z_i is the laser point elevation value, and h_i is the elevation value of the DSM generated from satellite images of the corresponding path. With this condition, the minimum elevation difference alignment can be constructed to obtain the best matching position of the photon profile point cloud strips relative to the direction of the satellite image-generated DSM trajectory, so as to obtain the overall offset of its spatial position.

The slope of the terrain is used as the basic discriminator, which is an important indicator to describe the terrain features and can indirectly reflect the relief pattern and structure of the terrain. For discrete photon point cloud data, a Gaussian fitting method is used to fit the curve, which can obtain more reliable terrain feature points. Then the terrain feature points are extracted from the elevation profile of the satellite-borne photon point cloud tracks based on the slope change, and all the terrain feature points with slope change values larger than the threshold are automatically labeled by setting the slope change threshold as the criterion. Take ICESat-2 point cloud data as an example, the extraction effect is shown in **Figure 13**. The continuous photon point cloud forms the terrain profile, and after the Gaussian curve fitting, it forms a smoother curve.

The principle of laser terrain feature point joint satellite image geolocation is to introduce the laser point as the control condition into the RFM compensation equation, to solve the problem that the parameters to be solved as free unknowns under the uncontrolled condition will lead to unstable accuracy of adjustment [68–75]. The basic process is to firstly match the connection points of satellite images and perform the free network adjustment; then bring the joint topographic feature points as the plane-height
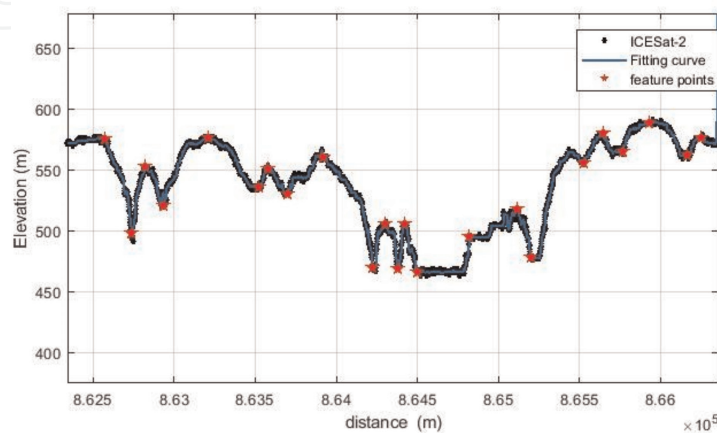

Figure 13.
Terrain feature points extracted from the photon profile point cloud.

control condition into the block adjustment of satellite images with additional parameters, and different weights be set to participate in the adjustment according to the observation accuracy of different data until the iterative calculation converges; finally, count the adjustment accuracy and output the adjustment results, i.e., the refined image positioning parameters, including RFM model coefficients and additional parameters, which are used together to realize the improvement of satellite image positioning accuracy. The characteristics of this adjustment scheme are that, due to the dense and continuous data of photon point cloud flight, it provides the possibility to automatically extract the topographic features common to both laser and stereo images with active and passive 3D observation data, thus providing an effective way to determine the position of photon point cloud on non-synchronous images, which enables its advantages of both plane and elevation accuracy to be fully exploited.

Comparing the results of uncontrolled, SRTM DEM-assisted and ICESat-2 control points, the uncontrolled block adjustment is based only on the self-contained rational function model, with a plane positioning accuracy of 8.12 m and an elevation accuracy of approximately 8.99 m. By introducing 5 m resolution open-source DOM and open 30 m grid spacing SRTM elevation data, and adding certain accuracy of plane and elevation geometric constraints, the accuracy of SRTM-assisted stereo image positioning is 6.65 m in plane and 2.019 m in elevation. When 1-track ICESat-2 laser point cloud control points are added to the test area, the 3D positioning accuracy of the image can be significantly improved to 2.64 m in plane and 1.39 m in elevation. Compared with the fully uncontrolled positioning and SRTM data-assisted positioning methods, the planimetric accuracy improved from 8.12 m, 6.65 m to 2.56 m, and the elevation accuracy improved from 8.99 m, 2.019 m to 1.319 m, with an improvement of 61.5% and 34.8% respectively compared with SRTM data. In the results from **Table 2**, we can see that the photonic laser point cloud can provide sufficient number of control point data, and the accuracy of auxiliary satellite stereo image positioning can reach the design theoretical accuracy.

The satellite-borne photonic point cloud has new breakthroughs in improving the positioning accuracy of satellite images compared with the existing linear system laser altimetry data and open-source global DEM: first, as a control of the adequacy of data distribution; second, the improvement of data accuracy, especially planimetric accuracy. This all provides a new technology path for achieving global accurate mapping.

Ground control	Image error	L-GCP's number	Check point	Planimetric error (m)	Elevation error (m)
Non-ground control	0.629			8.12	8.99
SRTM	0.330			6.65	2.019
1-Track photon point clouds	0.328	10	5	2.68	1.450
	0.326	18	7	2.64	1.390
5-Track photon point clouds	0.325	10	50	2.57	1.325
	0.325	15	73	2.56	1.319

Table 2.
Accuracy statistics of uncontrolled block adjustment and auxiliary block adjustment.

5.2 Multi-source topographic information fusion

Obtaining high accuracy, high resolution, and global coverage, Digital Elevation Model (DEM) is the goal of aerospace remote sensing mapping [76]. The existing open-source DEM mainly includes SRTM (Shuttle Radar Topography Mission), GDEM (Global Digital Elevation Model), etc. GDEM is an elevation model acquired by Terra satellite optical sensor ASTER with 30 m resolution, covering about 99% of the global land surface. The SRTM is a Space Shuttle radar topographic mapping product with the latest release being the 30 m resolution SRTM-1. GDEM and SRTM-1 have nominal elevation accuracies of 17 m (95% confidence) and 16 m (90% confidence), respectively [77, 78]. In comparison, GDEM has noise and data artifacts due to optical imaging limitations, and SRTM has stable accuracy but data gaps at large slope locations in mountainous areas. ICESat-2 elevation accuracy is much higher than these two open DEMs, while the point density along the track direction is extremely high, and the ICESat-2 point cloud can be used as a control point to correct the open-source DEM elevation deviation and ensure the quality of DEM blank filling [79–82].

Specific processing should pay attention to the unification of coordinate system and elevation datum, ICESat-2 ATL03 point cloud coordinate system is WGS84, the elevation value is ellipsoidal height, the file provides the elevation aberrant value under EGM08 (Earth Gravitational Model 2008) (field/gtx/geophys_corr/geo), which can be read and converted to normal elevation. Corrected DEMs are evaluated with ICESat-2, which allows the mapping of laser points to open-source DEM values to be established and corrections carried out. Vacancy filling is achieved through steps such as rasterization, interpolation (e.g., inverse distance weights, kriging, etc.) [83, 84] and triangulated mesh surface filling. The method that SRTM-1 and GDEM fusion filling were supported by ICESat data has been shown to be effective, and the evaluation shows that the accuracy of GDEM, SRTM-1, and ICESat after fusion processing is 10.9 ± 20.2, 5.8 ± 16.2, and 5.7 ± 14.9 m, respectively, and ICESat-2 is theoretically better for fusion processing.

As shown in **Figure 14**, the results of the fusion processing of multi-source terrain information supported by the strip control datum are used. For the differences of shift and rotation between multiple topographic data in the same area, a fusion processing
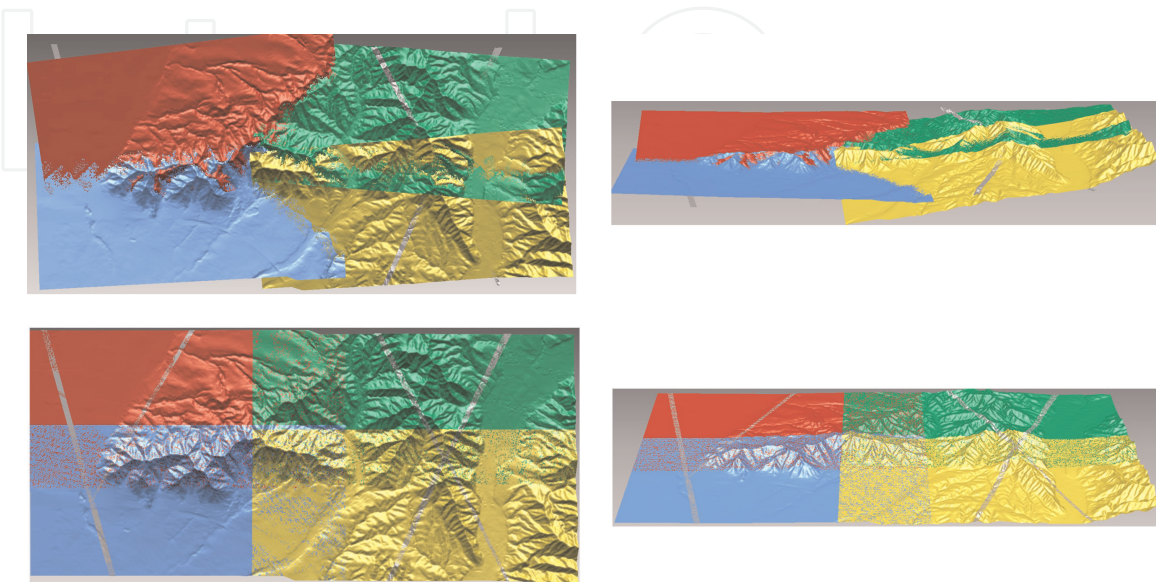

Figure 14.
Comparison of the before-after fusion of multi-source topographic data (top view and side view).

method consisting of ICP topographic matching, spatial geometric transformation overall adjustment, and topographic reconstruction is proposed, and the experimental results show that the method can effectively eliminate the systematic geometric errors between different topographic data and improve the fusion accuracy of multi-source topographic data. At the same time, because the terrain matching depends on the terrain features, the feature matching accuracy is better when the terrain is highly rolling, and the overall adjustment accuracy is also better in mountainous or hilly areas compared with flat areas.

5.3 Polar mapping

In recent years, polar ice sheet mass balance studies have revealed that the Antarctic and Greenland ice sheets as a whole are in a state of accelerated melting, which has important implications for both global sea level rise and climate change [85, 86]. Satellite laser altimetry, represented by ICESat-2, is an important tool for mapping changes in polar ice sheet elevation and thus analyzing the ice sheet material balance [87–90].

Mapping polar ice cap elevation changes is one of the main scientific objectives of ICESat-2. At present, the main methods for mapping the elevation change of the polar ice cap surface using ICESat-2 include the intersection point method and the repeated trajectory method. The former uses multiple functions to fit the satellite lift orbits and calculate the ice cap elevation change at the orbit intersection points and their locations. The latter method divides the satellite orbit into kilometer-scale segments and uses least squares to fit the segment function model to calculate the ice cap elevation change. Compared with the traditional single-beam measurement mode used by ICESat, the multi-beam measurement of ICESat-2 greatly increases the number of intersections and effectively improves the ability to obtain details of the ice cap surface elevation change. At the same time, ICESat-2's paired laser beams can independently determine the local surface slope, making it possible to determine surface elevation changes using a single repeated reference track.

ICESat-2 features multiple beams, high repetition frequency, and micro-pulses, which greatly enhance the accuracy and reliability of polar observation results. On the spatial scale of 100 km^2, ICESat-2 has an accuracy of better than 0.25 m/year for ice sheet elevation change measurements and can provide high-precision observations of better than 0.4 cm/year over the entire Antarctic or Greenland ice sheets [53]. **Figure 15** shows the Greenland ice sheet elevation change from 2003 to 2019 based on the intersection of ICESat and ICESat-2. The high-resolution and high-precision measurements provided by ICESat-2 will greatly improve the mapping accuracy in the ice sheet edge areas with large topographic relief and provide more reliable data support for the analysis of the polar ice sheet material balance.

5.4 Three-dimensional topographic mapping

The satellite-based laser survey can quickly and accurately acquire three-dimensional information on the earth's surface, providing a new means for terrestrial elevation three-dimensional mapping. Due to the high altitude of the satellite platform, unlike the airborne platform scanning measurement mode, the satellite-based LiDAR measurement adopts a multi-beam push measurement mode similar to the optical remote sensing satellite line array push imaging. Although the photon counting point cloud data in the flight direction forms a continuous surface elevation profile
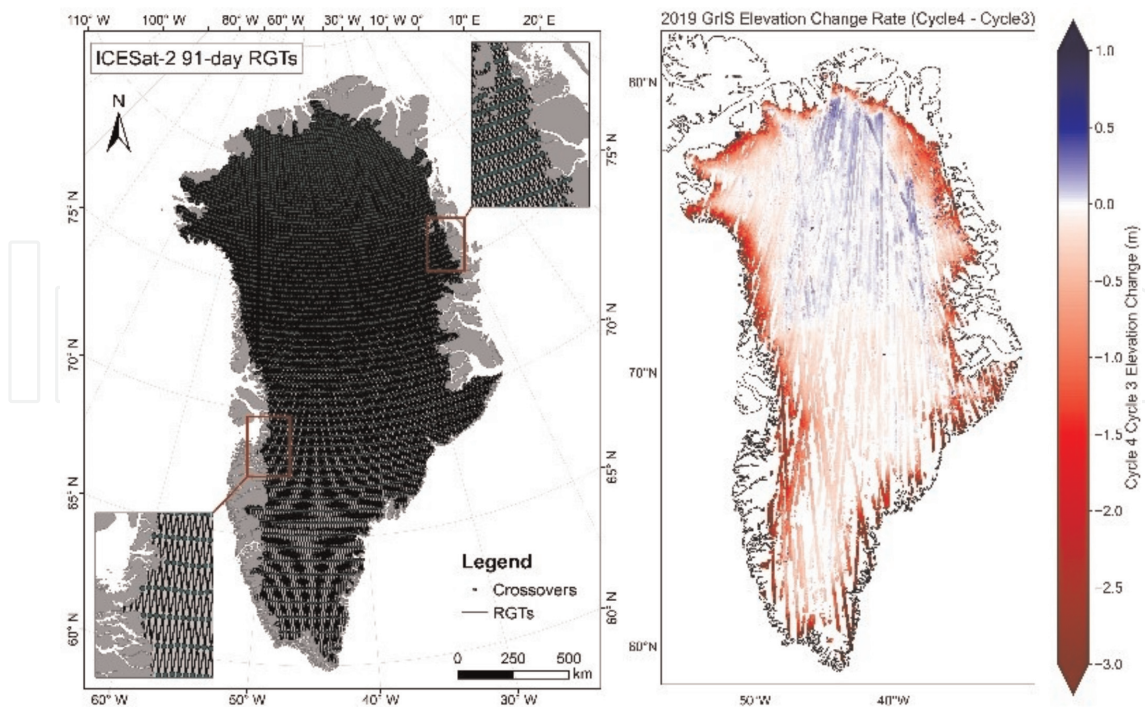
Figure 15.
Changes in the elevation of the Greenland ice sheet from 2003 to 2019 based on the intersection of ICESat and ICESat-2.

due to high sampling frequency, and the ground sampling distance can reach sub-meter level, the sampling interval in the vertical orbit direction may reach hundreds to thousands of meters in magnitude due to the limitation of the number of beams, and the sampling spacing between the two directions is large, making it difficult to effectively measure the object shape. Icesat-2, for example, has a sampling interval of 0.7 meters in the along-track direction and more than 3.3 kilometers in the vertical-track direction, so it is difficult to meet the requirements of three-dimensional terrain mapping with a single pass, which limits the scope of application.

However, as the satellite cycle operation can realize the same area repeatedly observed several times, the sampling distance between sparse beams is gradually reduced, and the point cloud data interval in the vertical track direction can be effectively reduced by using joint processing of multi-track data, **Figure 16** shows the results of multi-track photon counting point cloud data processing using airborne 51-beam LiDAR. The sampling interval between the two directions gradually converges to the same, and finally realizes 3D mapping of the surface object, which can provide a better data source for 3D model reconstruction.

The simulation of satellite operation by airborne experiment shows that although the laser points are widely spaced in the vertical orbit direction, the dense point cloud with more uniform distribution can be obtained by multi-track coverage, which can better reflect the three-dimensional shape of the ground surface. Further, the laser point cloud can be filtered and classified, and a typical algorithm such as the adaptive progressive triangular network filtering method can classify the point cloud into two categories: ground points and non-ground points. Then, according to the spatial distribution of non-ground points, they are further divided into buildings, vegetation and others. In the case of building point clouds, RANSAC plane detection and clustering as well as key point/corner point and boundary extraction are used to achieve automatic reconstruction of
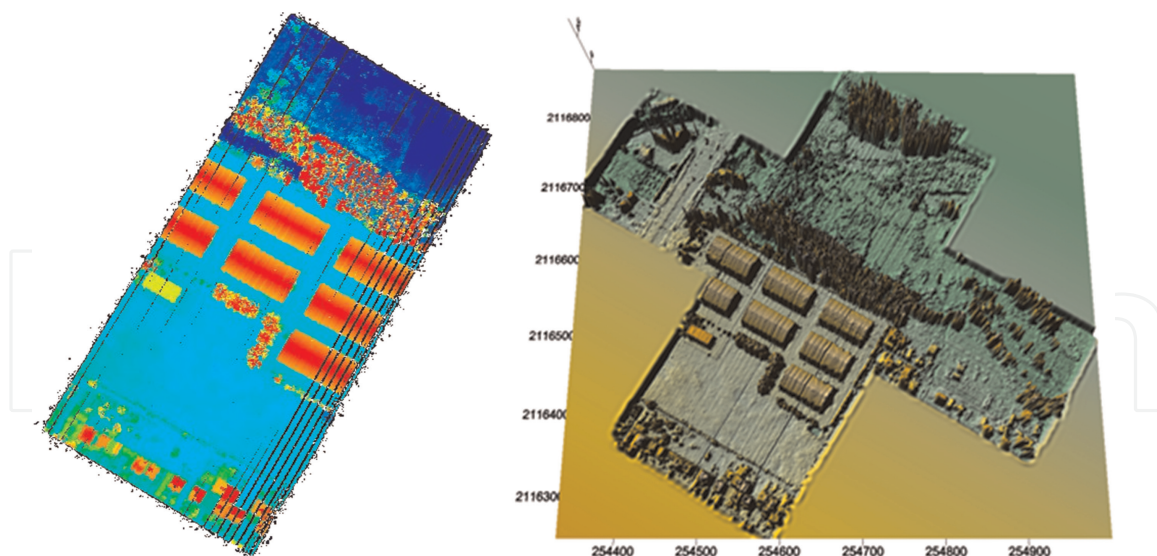
Figure 16.
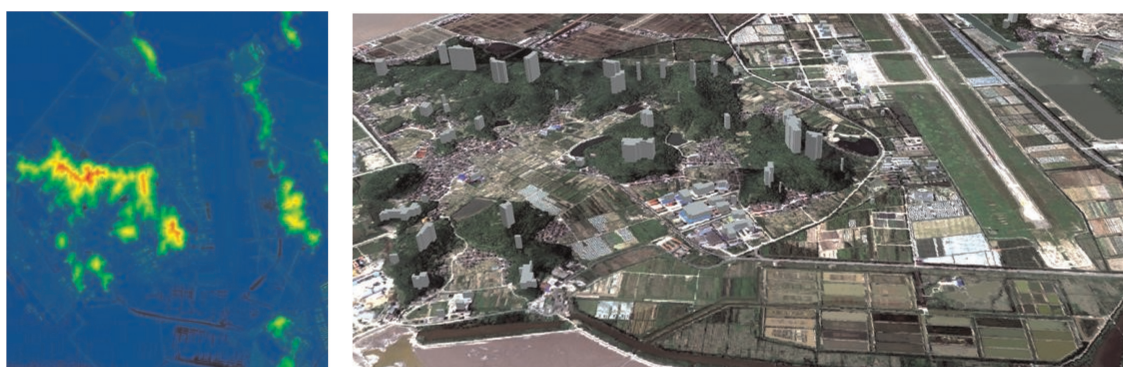*Airborne multi-orbit photon counting point cloud data and processing results.*

Figure 17.
Automatic building extraction from 5m laser point cloud data and LOD1 level 3D reconstruction.

LOD1 level building 3D models, as shown in **Figure 17**, and higher detail levels require further integration of multi-source data such as high-resolution multi-view images, spectral information, geographic information and even mobile phone videos.

At the same time, in order to further improve the efficiency and fineness of the target 3D measurement, the combination of LiDAR measurement and oblique photogrammetry to achieve rapid 3D mapping of the target is an effective technical approach. At present, a payload device Leica CityMapper, which integrates two detection instruments, has emerged in the aerial photogrammetry field, collecting 3D city oblique photography images and laser point cloud data simultaneously, which can effectively improve the productivity and data quality of creating digital city 3D models, realizing efficient and low-cost acquisition of highly detailed and accurate 3D data, and making the widespread use of 3D models a reality. This provides a good reference for the design of a satellite-based hybrid 3D mapping system.

5.5 Shallow Sea topographic mapping

Shallow bathymetry is the basic geographic data required for many applications such as marine engineering construction and marine environmental research, and it is
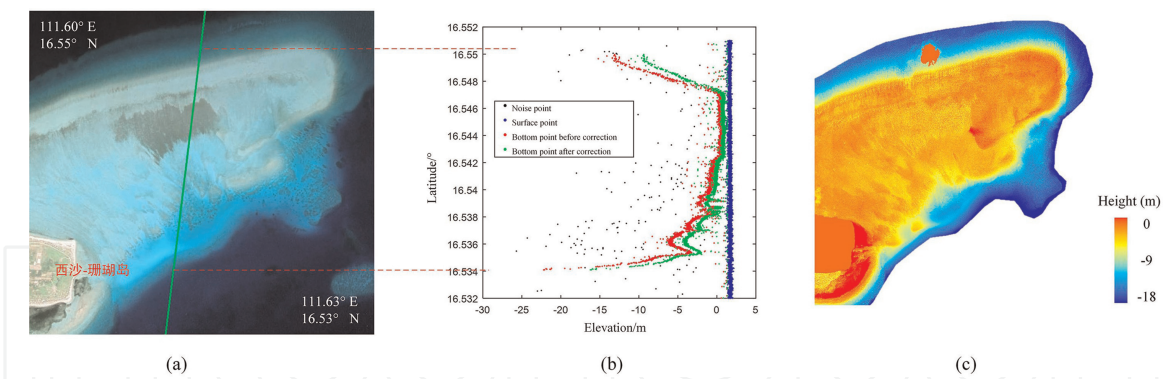
Figure 18.
Schematic diagram of ICESat-2 shallow bathymetry. (a) Geographical location of Xisha Coral Island; (b) ICESat-2 photon profile point cloud and refraction correction effect; (c) shallow water deep pseudo-color map.

a difficult and hot spot in the field of marine mapping to obtain shallow bathymetry accurately and efficiently [91–93].

Laser propagation has to go through a complex process of atmosphere-water body-atmosphere, and the returned laser energy is significantly weakened due to the attenuation of the water body, it is difficult for satellite platforms to detect shallow water depth in the linear detection laser stage, and the ultra-high sensitivity of photon-counting LiDAR makes it a reality. The on-board experimental results of MABEL (ICESat-2 principle prototype) show that the laser bathymetry depth reaches 8 m with a root mean square error 0.7 m [94]; after the release of ICESat-2 data, analysis showed a maximum bathymetric depth of up to 40 m with a root mean square error in the range of 0.43–0.6 m [53]. **Figure 18** shows the joint bathymetry test with World-View-2 optical images using ICESat-2 at the Xisha coral reef in China, with an accuracy of 0.23 ± 0.98 m. It should be noted that the standard product released by ICESat-2 does not have shallow bathymetry, i.e., the elevation value of ATL03 point cloud does not take into account the refraction of the water body, so the practical application needs to carry out targeted denoising, refraction correction, surface/submerged separation, and bathymetry calculation; at the same time, due to the large spacing of ICESat-2 beam vertical tracks, many distant islands and reefs are not passed by the survey line, so the joint processing of laser and image in a certain range to carry out water body inversion parameter transposition is a more feasible method for the area lacking direct active bathymetry values.

6. Conclusions

The rapid development of satellite-based LiDAR earth observation technology provides an effective way to rapidly collect global surface 3D point clouds, and the advantages and characteristics of laser point cloud data make it a core data component for the construction of the next-generation global mapping database, establishing an infrastructure for the construction of high-precision global control grids and highly efficient surveying of digital elevation maps, and providing support for the rapid construction of high-precision 3D digital geospatial frameworks. At the same time for the global laser point cloud application needs and overall design, it is also necessary to strengthen the research to continuously optimize the technical process, focusing on the following aspects:

1. Global point cloud density. Laser measurements are similar to field measurements in that they are single point measurements, but due to the disorderly nature of laser point cloud data, different applications have corresponding requirements for point cloud density. For regional/national airborne point cloud density is generally 6–10 points/m^2, for example, for the whole of Finland, the area is 338,000 km^2, there are 640 billion points, and the data volume is about 11 TB, while for ground mobile LiDAR point cloud data, the density may exceed 1000 points/m^2. In general, point cloud density is closely related to the application environment. For the global three-dimensional framework construction, the current satellite laser point cloud spacing of 5–10 m should be a reasonable interval, taking into account the mapping efficiency and satellite instrument performance.

2. Point cloud automated mapping. The extraction of multiple spatial information from the satellite-based point cloud data, including terrain, buildings, vegetation, etc., needs to further improve the degree of automation and accuracy, to provide effective support for the construction of three-dimensional digital geospatial information framework. Laser point cloud data automatically classifies ground points and non-ground points, and reliable ground points are the key to rapidly generate digital ground models; non-ground points contain structural information of surface targets, from which there is still a great challenge to automatically reconstruct the 3D framework model of ground targets.

3. Multi-sensor integration. In order to obtain finer surface 3D information, multi-sensor integration and fusion will be an inevitable choice for the development of satellite-based earth observation technology, to achieve the high accuracy of satellite-based LiDAR measurement data and the high resolution of optical/ microwave imaging technology combined to give full play to the advantages of multiple detection means [22, 95–97]. The need to study the automatic and accurate matching between LiDAR measurement data and imaging sensor data, as well as the overall fusion strategy for the difference in accuracy between the two, are issues that need to be further studied and solved.

4. Rapid application mode. Point cloud data are a discrete expression of the earth surface, directly superimposed orthophoto fast 3D display has a more intuitive visualization ability than only using vector maps, on the basis of which further superimposed thematic information can meet the rapid application needs in emergency situation. This mode has higher efficiency and flexibility compared with point cloud 3D model reconstruction. Therefore, it is necessary to pay attention to the development of technologies such as 3D game engines, including the host platform, development environment, and tools applicable to global point cloud data, as well as the construction and development of standard interfaces.

Since the first satellite-based laser altimetry satellite ICESat-1 was successfully launched in 2003, after nearly two decades of development, satellite LiDAR earth observation technology has achieved great progress and gradually developed into an emerging remote sensing exploration instrument. Especially since 2018, ICESat-2 satellite (2018), GEDI (2018), Gaofen-7 (2019), Gaofen-14 (2020), and terrestrial ecological environment monitoring carbon satellite (2022) have been continuously

launched into the sky, and the satellite laser observation technology has come to a climax of development. The update of acquiring tools has provided new opportunities for the global mapping technology, and studies have shown that spaceborne laser observation data have strong application potential in the fields of precise positioning of global earth, polar ice sheet monitoring, and shallow ocean topography mapping, etc. It is foreseen that in the near future, with the further development of satellite-based LiDAR technology, it will become possible to directly acquire global digital surface models and digital elevation models, thus providing an active technical way to establish uniformly accurate elevation data in a global even grid, and a new means to establish a higher precision 3D digital earth model.

Author details

Fang Yong*, Zhang Li, Gong Hui, Cao Bincai*, Gao Li and Hu Haiyan
Xi'an Research Institute of Surveying and Mapping, Xi'an, China

*Address all correspondence to: yong.fang@vip.sina.com and cbontheway@163.com

IntechOpen

References

[1] Li DR. From geomatics to geospatial intelligent service science. Acta Geodaetica et Cartographica Sinica. 2017;**46**(10):1207-1212

[2] Juho-Pekka V, Antero K, Harri K, etc. Nationwide point cloud-the future topographic Core data. ISPRS International Journal of Geo-Information. 2017;**6**(8):243

[3] Li R, Wang C, Su GZ, et al. Development and application of spaceborne lidar. Science & Technology Review. 2007;**14**:58-63

[4] Yu ZZ, Hou X, Zhou CY. Development status of spaceborne laser altimetry technology. Laser & Optoelectronics Progress. 2013;**50**(02): 52-61

[5] Fang Y, Cao BC, Gao L, et al. Development and application of lidar mapping satellite. Infrared and laser engineering. 2020;**49**(11):19-27

[6] Zhu XX, Wang C, Xi XH, et al. Research progress on data processing and application of icesat-2 spaceborne photon counting lidar. Infrared and Laser Engineering. 2020;**49**(11):76-85

[7] Fang Y. Research and Practice of Spaceborne SAR Image Spatial Information Extraction Technology. Zhengzhou: Zhengzhou University of Information Engineering; 2001

[8] Fang Y, Gong H, Zhang L, Haiyan H. From global laser point cloud acquisition to 3D digital geospatial framework: The advanced road of global accurate mapping. Laser & Optoelectronics Progress. 2022;**59** (12):1200002 (in Chinese)

[9] Xin X, Liu B, Di K, Yue Z, Gou S. Geometric quality assessment of

Chang'e-2 global DEM product. Remote Sensing. 2020;**12**(3):526-546

[10] He Y. Research on Lunar Topography Mapping Technology Based on Lunar CCD Image and Laser Altimetry Data. Zhengzhou: PLA University of Information Engineering; 2012

[11] Hu H, Wu B. Planetary 3D: A photogrammetric tool for 3D topographic mapping of planetary bodies. The ISPRS Annals of the Photogrammetry, Remote Sensing and Spatial Information Sciences. 2019; **IV-2/W5**:519-526. DOI: 10.5194/isprs-annals-IV-2-W5-519-2019

[12] Guoyuan L. Earth Observing Satellite Laser Altimeter Data Processing Method and Engineer Practice. Wu Han: Wu Han University; 2017 (in Chinese)

[13] Sun G, Ranson KJ, Kharuk VI, et al. Validation of surface height from shuttle radar topography mission using shuttle laser altimeter. Remote Sensing of Environment. 2003;**88**(4):401-411

[14] Simard M, Pinto N, Fisher J, et al. Mapping forest canopy height globally with spaceborne lidar. Journal of Geophysical Research. 2011, 2011; **116**(G4):1-12

[15] Scott BL, Tim R, Taylor T, et al. Algorithm Theoretical Basis Document (ATBD) for GEDI Waveform Geolocation for L1 and L2 products. [EB/OL]. 2019. Available from: http://lpdaac.usgs.gov/documents/579/GEDI_WFGEO_ATBD_v1.0.pdf [Accessed: October 24, 2022]

[16] Xinming T, Junfeng X, Xinke F, et al. ZY3-02 laser altimeter on-orbit

geometrical calibration and test. Acta Geodaetica et Cartographica Sinica. 2017;**46**(6):714-723 (in Chinese)

[17] Chen GD, Wang P, Zhao W. ICESat ice sheet height measurement accuracy estimation based on intersection mismatch. Journal of Surveying and Mapping Science and Technology. 2018; **35**(03):226-230

[18] Hu GJ, Fang Y, Zhang L. Development of spaceborne lidar and analysis of surveying and mapping application prospect. Surveying and Mapping Technology and Equipment. 2015;**17**(02):34-37

[19] Chen BX, Zhu Q, Hu H. ZY-3 global DEM accuracy evaluation method based on glas laser altimetry data. Geographic Information World. 2019;**26**(06):70-73

[20] Wei ZQ. Pay attention to ICESat. In: Proceedings on the Progress of Geodesy and Geodynamics. HuBei Science and Technology Press; 2004. pp. 41-44

[21] Li GY, Tang XM, Zhang CY, et al. Multi-criteria constraint algorithm for selecting ICESat/GLAS data as elevation control points. Journal of Remote Sensing. 2017;**21**(1):96-104

[22] Wang J, Zhang Y, Zhang ZX, et al. ICESat laser points assisted block adjustment for mapping Satellite-1 stereo imagery. Acta Geodaetica et Cartographica Sinica. 2018;**47**(3): 359-369

[23] Zhang ZX, Tao PJ. An overview on "cloud control" photogrammetry in big data era. Acta Geodaetica et Cartographica Sinica. 2017;**46**(10): 1238-1248

[24] Tang XM, Xie JF, Mo F, et al. GF-7 dual-beam laser altimeter on-orbit geometric calibration and test

verification. Acta Geodaetica et Cartographica Sinica. 2021;**50**(3): 384-395

[25] Aiyan G, Jun D, Chengguang Z, et al. Design and on-orbit validation of GF-7 satellite laser altimeter. Spacecraft Engineering. 2020;**39**(3):43-48 (in Chinese)

[26] Leigh HW, Magruder LA, Carabajal CC, et al. Development of onboard digital elevation and relief databases for ICESat-2. IEEE Transactions on Geoscience & Remote Sensing. 2015; **53**(4):2011-2020

[27] Gong P, Huang HB. The application prospect of lidar technology in topographic mapping in China. Geographic Information World. 2008; **6**(06):45-48

[28] Cao BC, Fang Y, Gao L, et al. Verification of ICESat-2/ATLAS laser altimetry data accuracy by airborne point cloud detection. Journal of Surveying and Mapping Science and Technology. 2020;**37**(01):50-55

[29] Abdalati W, Zwally HJ, Bindschadler R, et al. The ICESat-2 laser altimetry mission. Proceedings of the IEEE. 2010; **98**(5):735-751

[30] Ma Y. Data Processing and Error Analysis of Spaceborne Laser Altimetry System. Wuhan: Wuhan University; 2013

[31] Li X, Liao H, Zhao ML, et al. Research on LiDAR surveying satellite detection capacity for different terrains. Acta Geodaetica et Cartographica Sinica. 2014;**43**(12):1238-1244

[32] Li S, Xiao JM, Ma Y, et al. Study on atmospheric refraction delay correction model of spaceborne laser altimetry

system. Optics and Optoelectronics Technology. 2013;**11**(01):7-11

[33] Yi H, Li S, Ma Y, et al. On orbit calibration of laser altimeter based on footprint detection. Acta Physica Sinica. 2017;**66**(13):118-126

[34] Li M. Research on Photon Counting Lidar Technology Based on fiber Optics. Beijing: University of Chinese Academy of Sciences; 2017

[35] Guo Y. Research on Key Technologies of Photon Counting 3D imaging Lidar. Beijing: Graduate School of Chinese Academy of Sciences; 2011

[36] Cao BC, Fang Y, Gao L, et al. Implementation and accuracy evaluation of ICESat-2 ATL08 denoising algorithms. Bulletin of Surveying and Mapping. 2020;(5):25-30 (in Chinese)

[37] Neumann TA, Martino AJ, et al. The ice, cloud, and land elevation Satellite-2 mission: A global geolocated photon product derived from the advanced topographic laser altimeter system. Remote Sensing of Environment. 2019;**233**:111325

[38] Dong J, Ni W, Zhang Z, Sun G. Performance of ICESat-2 ATL08 product on the estimation of forest height by referencing to small footprint LiDAR data. National Remote Sensing Bulletin;**25**(6):1294-1307

[39] Sun W, Jin J, Li G, Yao J. Accuracy evaluation of laser altimetry satellite ICESat-2 in monitoring water level of Taihu lake. Science of Surveying and Mapping. 2021;**46**(11):6-11

[40] Zhu X, Wang C, Xi X, Nie S, Li D. Research progress of ICESat-2/ATLAS data processing and applications. Infrared and Laser Engineering. 2020;**49**(11):76-85

[41] Neuenschwander AL, Magruder LA. Canopy and terrain height retrievals with ICESat-2: A first look. Remote Sensing. 2019;**11**(14):1721

[42] Bentley Pointools: Point-Cloud Processing Software. Available from: https://www.bentley.com/en/products/product-line/reality-modeling-software/bentley-pointools [Accessed: October 24, 2022]

[43] Euclideon Udstream. Available from: https://www.euclideon/udstream/ [Accessed: October 24, 2022]

[44] Li G, Ye F, Tang X, et al. Influence of range gate width on detection probability and ranging accuracy of single photon laser altimetry satellite. Journal of Geodesy and Geoinformation Science. 2020;**3**(2):36-44

[45] Cao B, Fang Y, Gao L, Hu H, Jiang Z. Verification of ICESat-2/ATLAS laser altimetry data accuracy using airborne point cloud. Journal of Geomatics Science and Technology. 2020;**37**(01): 50-55

[46] Neumann T, Brenner A, Hancock D, et al. NASA. ICE, CLOUD, and Land Elevation Satellite (ICESat-2) Algorithm Theoretical Basis Document (ATBD) for Global Geolocated Photons ATL03 [EB/OL] 2019. Available from: https://icesat-2.gsfc.nasa.gov/sites/default/files/page_files/ICESat2_ATL03_ATBD_r001.pdf [Accessed: 25 August 2020]

[47] Neuenschwander A, Pitts K. ICE, CLOUD, and Land Elevation Satellite (ICESat-2) Algorithm Theoretical Basis Document (ATBD) for Land - Vegetation Along-track products (ATL08) [EB/OL]. 2019. Available from: https://icesat-2.gsfc nasa.gov/sites/default/files/page_files/ICESat2_ATL08_ATBD_r001_0.pdf [Accessed: 25 August 2020]

[48] Neuenschwander A, Pitts K. The ATL08 land and vegetation product for the ICESat-2 Mission. Remote Sensing of Environment. 2019;**221**:247-259

[49] Feng X, Gui Y, Rong S, et al. An adaptive directional filter for photon counting lidar point cloud data. Journal of Infrared, Millimeter, and Terahertz Waves. 2017;**36**(1):107-113 (in Chinese)

[50] Xie J, Liu R, Mei Y, et al. Preliminary pointing bias calibration of ZY3-03 laser altimeter. Journal of Geodesy and Geoinformation Science. 2021;**4**(3): 91-100

[51] Tang X, Li G, Gao X, Chen J. The rigorous geometric model of satellite laser altimeter and preliminarily accuracy validation. Acta Geodaetica et Cartographica Sinica. 2016;**45**(10): 1182-1191

[52] Nan YM, Feng ZH, Liu EH, et al. Iterative pointing angle calibration method for the spaceborne photon-counting laser altimeter based on small-range terrain matching. Remote Sensing. 2019;**11**(18):2158

[53] Markus T, Neumann T, Martino A, et al. The ice, cloud, and land elevation Satellite-2 (ICESat-2): Science requirements, concept, and implementation. Remote Sensing of Environment. 2017;**190**:260-273

[54] Marco GMS. Automated geometric correction of high-resolution Pushbroom satellite data. Photogrammetric Engineering & Remote Sensing. 2008; **74**(1):107-116

[55] Reinartz P et al. Orthorectification of VHR optical satellite data exploiting the geometric accuracy of TerraSAR-X data. ISPRS Journal of Photogrammetry and Remote Sensing. 2011;**66**(1):124-132

[56] Zhou P, Tang X, Cao N, Wang X, Li G, Zhang H. SRTM-aided stereo image block adjustment without ground control points. Acta Geodaetica et Cartographica Sinica. 2016;**45**(11):1318-1327

[57] Di K, Liu B, Peng M, et al. An initiative for construction of new-generation lunar global control network using multi-mission data. ISPRS— International Archives of the Photogrammetry, Remote Sensing and Spatial Information Sciences. 2017; **XLII-3/W1**:29-34

[58] Cao H, Tao P, Li H, Shi J. Bundle adjustment of satellite images based on an equivalent geometric sensor model with digital elevation model. ISPRS Journal of Photogrammetry and Remote Sensing. 2019;**156**:169-183

[59] Wang M, Wei Y, Yang B, Zhou X. Extraction and analysis of icesAT-2/ ATLAS global elevation control points. Geomatics and Information Science of Wuhan University. 2021;**46** (2):184-192

[60] Hanley HB, Yamakawa T, Fraser CS. Sensor orientation for high-resolution satellite imagery. In: International Archives of Photogrammetry and Remote Sensing. No. 34. 2002

[61] Toutin T. Spatiotriangulation with multisensor VIR/SAR images. IEEE Transactions on Geoscience and Remote Sensing. 2004;**42**(10):2096-2103

[62] Liu S, Lv Y, Tong X, et al. An alternative approach for registration of high-resolution satellite optical imagery and ICESat laser altimetry data. Sensors. 2016;**16**(12):2008

[63] Li G, Tang X. Analysis and validation of ZY-3 02 satellite laser altimetry data.

Acta Geodaetica et Cartographica Sinica. 2017;**46**(12):1939-1949

[64] Li G. Earth observing satellite laser altimeter data processing method and engineer practice. Acta Geodaetica et Cartographica Sinica. 2018;**47**(12): 1691-1691

[65] Li G, Tang X, Gao X, et al. Improve the ZY-3 height accuracy using icesat\glas laser altimeter data. The International Archives of the Photogrammetry, Remote Sensing and Spatial Information Sciences. 2016;**XLI-B1**:37-42

[66] Li G, Wang Y, et al. ZY-3 block adjustment supported by glas laser altimetry data. Photogrammetric Record. 2016;**31**(153):88-107

[67] Lai WY, Fang Y. Block adjustment of satellite images supported by spaceborne photon point cloud. Laser & Optoelectronics Progress. 2023;**60**(10): 1028013

[68] Grodecki J, Dial G. Block adjustment of high-resolution satellite images described by rational polynomials. Photogrammetric Engineering & Remote Sensing. 2003;**69**(1):59-68

[69] Yang B, Wang M, Pi Y. Block-adjustment without GCPs for large-scale regions only based on the virtual control points. Acta Geodaetica et Cartographica Sinica. 2017;**46**(7):874-881

[70] Li G, Tang X, Wang H, et al. Research on the ZY-3 block adjustment supported by the GLAS laser altimetry data. In: The 3rd Annual Academic Conference on High Resolution Earth Observation. 2014. pp. 586-600

[71] Wang J, Zhang Y, Zhang Z, et al. ICESat laserpoints assisted block adjustment for mapping satellitle-1 stereo imagery. Acta Geodaetica et Cartographica Sinica. 2018;**47**(03): 359-369

[72] Cao N, Zhou P, Wang X, et al. Refined processing of laser altimeter data-aided satellite geometry model. Journal of Remote Sensing. 2018;**22**(4):599-610

[73] Tang X, Liu C, Zhang H, Wang X, Guoyuan L, Mo F, et al. GF-7 satellites stereo images block adjustment assisted with laser altimetry data. Geomatics and Information Science of Wuhan University. 2021;**46**(10):1423-1430

[74] Cai C. Research on ICESat-2 Point Cloud Data Assisted Satellite Image DEM Extraction Method. XiAn: Chang'an University; 2020

[75] Zhang L, Xing S, Xu Q, Zhang G, Li P, Jiao L, et al. Joint block adjustment for ATLAS data and ZY3-02 stereo imagery. Infrared and Laser Engineering. 2020; **49**(S2):155-162

[76] Han H, Ding YL, Zhu Q, et al. Precision global DEM generation based on adaptive surface filter and poisson terrain editing. Acta Geodaetica et Cartographica Sinica. 2019;**48**(3): 374-383

[77] Li ZH, Li P, Ding D, et al. Research progress of global high resolution digital elevation models. Geomatics and Information Science of Wuhan University. 2018;**43**(12):1927-1942

[78] Yue L, Shen H, Zhang L, et al. High-quality seamless DEM generation blending SRTM-1, ASTER GDEM v2 and ICESat/GLAS observations. ISPRS Journal of Photogrammetry and Remote Sensing. 2017;**123**:20-34

[79] Hossein A, Peter R. Accuracy enhancement of ASTER global digital elevation models using ICESat data. Remote Sensing. 2011;**3**(7):1323-1343

[80] Yang S, Yang N, Chen C, et al. Accuracy assessment and improvement of SRTM DEM based on ICESat/GLAS under the consideration of data coregistration over Jiangxi Province. Journal of Geo-information Science. 2021;**23**(5):869-881

[81] Chen B, Zhu Q, Hu H. Global DEM accuracy evaluation method based on GLAS laser altimetry data. Geomatics World. 2019;**26**(6):70-73

[82] Zhang T, Cen M, Feng Y, Yang R, Ren Z. DEM matching algorithm using least trimmed squares estimator. Acta Geodaetica et Cartographica Sinica. 2009;**38**(2):144-151

[83] Shan J, Deng F, Tao PJ, et al. Crowdsource Image Photogrammetry [M]. Beijing: Science Press; 2019. pp. 49-73

[84] Wang X, Holland DM, Gudmundsson GH. Accurate coastal DEM generation by merging ASTER GDEM and ICESat/GLAS data over Mertz glacier, Antarctica. Remote Sensing of Environment. 2018;**206**: 218-230

[85] Li Q, Ke C, Zhang J, Xiaoyi S. Estimation of the mass balance of Greenland IceSheet from 2003 to 2019 based on ICESat and ICESat-2 laser altimetry data. Journal of Geo-information Science. 2022;**24**(3): 558-571

[86] Shepherd A, Ivins E, Rignot E, et al. Mass balance of the Antarctic ice sheet from 1992 to 2017. Nature. 2018; **558**(7709):219-222

[87] Gao XM, Li GY, Guo JQ, et al. Discussion on the development of three pole observation laser altimetry satellite. Infrared and Laser Engineering. 2020; **49**(11):40-46

[88] Luthcke SB, Rowlands DD, Williams TA, et al. Reduction of ICESat systematic geolocation errors and the impact on ice sheet elevation change detection. Geophysical Research Letters. 2005; **32**(21):1-4

[89] Brunt KM, Neumann TA, Smith BE. Assessment of ICESat-2 ice sheet Surface Heights, based on comparisons over the interior of the Antarctic ice sheet. Geophysical Research Letters. 2019; **46**(22):13072-13078

[90] Csatho BM, Schenk AF, Van Der Veen CJ, et al. Laser altimetry reveals complex pattern of Greenland Ice Sheet dynamics. Proceedings of the National Academy of Science of the United States of America. 2014;**111**(52):18478-18483

[91] Cao B, Fang Y, Gao L, Haiyan H, Jiang Z, Sun B, et al. An active-passive fusion strategy and accuracy evaluation for shallow water bathymetry based on ICESat-2 ATLAS laser point cloud and satellite remote sensing imagery. International Journal of Remote Sensing. 2021;**42**(8):2783-2806. DOI: 10.1080/ 01431161.2020.1862441

[92] Cao BC, Fang Y, Jiang ZZ, Gao L, Hu HY. Shallow water bathymetry from WorldView-2 stereo imagery using two-media photogrammetry. European Journal of Remote Sensing. 2019;**52**(1): 506-521

[93] Parrish CE, Magruder LA, Neuenschwander AL, et al. Validation of ICESat-2 ATLAS bathymetry and analysis of ATLAS's bathymetric mapping performance. Remote Sensing. 2019;**11**(14):1634

[94] Forfinski-Sarkozi N, Christopher P. Analysis of MABEL bathymetry in Keweenaw Bay and implications for ICESat-2 ATLAS. Remote Sensing. 2016; **8**(9):772

[95] Du QY, Mai XM, Chu FX, et al. Registration of unconventional aerial images and airborne lidar data based on ICP algorithm. Remote Sensing Information. 2014;**29**(06):16-20

[96] Cao BC, Fang Y, Jiang ZZ, et al. Bathymetry of icesat-2 laser satellite and optical remote sensing image fusion. Marine Surveying and Mapping. 2020;**40**(05):21-25

[97] He H, Wang ZM, Wen HF. Research on tilt correction of spaceborne SAR interferometric DEM using satellite laser altimetry data. Remote Sensing Information. 2009;**04**:85-88